

DOI: 10.1002/asia.201100849

Organic Dyes Containing Pyrenylamine-Based Cascade Donor Systems with Different Aromatic π Linkers for Dye-Sensitized Solar Cells: Optical, Electrochemical, and Device Characteristics

K. R. Justin Thomas,^{*,[a]} Neha Kapoor,^[a] Chuan-Pei Lee,^[b] and Kuo-Chuan Ho^[b]

Abstract: New organic dyes containing pyrenylamine donors in a cascade arrangement and cyanoacrylic acid acceptors have been synthesized and characterized by optical, electrochemical, and theoretical studies. The dyes inherit a D- π^1 -D- π^2 -A (D=donor, A=acceptor) molecular architecture where the π linkers π^1 are changed from phenyl to biphenyl and fluorene, whereas the π linker π^2 that connects the donor fragment with the acceptor is a phenyl unit. The conjugation pathway linking the two donor segments has been found to play a major role in

the optical and electrochemical properties. Shorter π linkers such as phenyl groups facilitate the donor-acceptor interaction while the nonplanar biphenyl spacer decreases the electronic communication between the donors and enhances the oxidation propensity of the corresponding dye. All the dyes display an intense longer wavelength electronic

transition, which is attributable to the amine-to-cyanoacrylic acid charge transfer. The extinction coefficient of this peak grows dramatically on increasing the conjugation pathway length between the two donor segments. The dyes were used as sensitizers in nanocrystalline TiO₂-based dye-sensitized solar cells (DSSCs) and the cascade donor system contributed to the enhancement in the device efficiency due to favorable absorption and redox properties.

Keywords: absorption • amines • density functional calculations • donor-acceptor systems • dye-sensitized solar cells

Introduction

Generation of electricity from alternative energy resources has gained immense attention in the past decade owing to the fear that fossil fuels might vanish rapidly as their consumption rate is growing year by year. Solar cells have been projected as an efficient alternative as the sun energy is available aplenty in most of the countries.^[1] Photoelectrochemical cells fabricated using organic dyes are commonly termed as organic solar cells (OSC) and have been considered as the cheaper alternative to the commercialized silicon-based solar cells.^[2] Organic solar cells based on nanocrystalline semiconductor oxides such as TiO₂ have been intensively studied in recent years owing to their low cost and their flexibility towards chemical modification, thus leading

to the tuning of functional properties.^[3] As the semiconductor oxide is not capable of absorbing the sun light by itself, organic dyes have been adsorbed on the surface of TiO₂ to extend their light-harvesting potential. Organic dyes containing donor-acceptor structural units linked by a suitable aromatic group and possessing a carboxylic acid group have been widely employed as sensitizers in excitonic solar cells.^[4] In most efficient dyes, the triarylamines served as donors while cyanoacrylic acid served as the acceptor.^[5-10] Efforts focused on the optimization of the functional efficacy of the organic dyes were directed to study the nature of donor or π -linker segments to find an effective dye. Organic dyes featuring various triarylamines and aromatic linkers such as oligophenyl,^[5] fluorene,^[6] carbazole,^[7] oligothiophene,^[8] coumarin,^[9] etc. have been developed and examined as sensitizers in dye-sensitized solar cells (DSSCs). Modification of the triarylamine chromophore by incorporation of electron-rich aromatic units such as fluorene has been found to be beneficial for enhancing the absorption properties and lowering the oxidation potential, which is necessary for the regeneration of the oxidized dye by the electrolyte.^[10] Incorporation of electron-rich segments in the conjugation pathway has been found to lower the excited-state ionization potential, which is essential for facilitating the electron injection into the conduction band of the TiO₂.^[11] Triarylamine-free organic dyes containing pyrenoidazole,^[12] phenanthrenoimidazole,^[13] imidazole,^[14]

[a] Dr. K. R. J. Thomas, N. Kapoor
Organic Materials Laboratory, Department of Chemistry
Indian Institute of Technology Roorkee
Roorkee—247 667 (India)
Fax: (+91) 1332-286202
E-mail: krjt8fcy@iitr.ernet.in

[b] C.-P. Lee, Prof. K.-C. Ho
Department of Chemical Engineering
National Taiwan University
Taipei 10617 (Taiwan)

Supporting information for this article is available on the WWW under <http://dx.doi.org/10.1002/asia.201100849>.

pyrene,^[15] fluorene,^[16] and/or thiophene^[17] have also been demonstrated as successful sensitizers.

Pyrene, a flat polyaromatic hydrocarbon possesses excellent fluorescence properties, carrier mobilities, and significant improved hole-injection ability than fluorene owing to its extended conjugation.^[18] Additionally, pyrene has an exceptionally long fluorescence lifetime in the range of 400 ns in deaerated solutions as compared to <10 ns observed for most organic fluorophores.^[19] Prolongation of excited-state lifetime will be beneficial for the excited-state processes such as electron-transfer reactions, and this is an essential criterion for the success of DSSCs. Though pyrene-based triarylamines^[20,21] and their polysubstituted derivatives^[22]

have been demonstrated as charge-transporting emitters and semiconductors in organic field-effect transistors (OFET), their use in photovoltaic devices is rather limited.^[6f] Thayumanavan and co-workers^[23] have used a pyrenylamino moiety as a donor in a dendritic donor–acceptor architecture and this showed an efficient photoinduced charge separation from the donor moiety to the benzothiadiazole-based acceptor unit. A dye with a pyrenylamine donor, 2-fluorenylthiophene linker, and a cyanoacrylic acid acceptor has been demonstrated as a sensitizer for DSSCs.^[6f] A series of pyrene end-capped organic dyes, with varying degree of conjugation linkers with cyanoacrylic acid, have been recently reported.^[15] However, to the best of our knowledge, systematic structure–property relationship studies on pyrenylamine donor-containing organic dyes suitable for DSSCs have not been undertaken. We have hypothesized that use of pyrenylamine units as donors in organic dyes will be useful for efficient charge separation due to their enhanced donor strength and enhanced excited-state lifetime and facile electron injection into the conduction band of TiO₂, owing to the favorable lowest unoccupied molecular orbital (LUMO). Thus, we have developed three dyes (Figure 1) containing two pyrenylphenylamine donor units in a cascade arrangement with aromatic segments with varying conjugation pathways such as phenyl, biphenyl, and fluorene. We have also synthesized two control dyes with a single donor unit to unravel the impact of the cascade donor system on the light-harvesting properties. The presence of additional donors in the DSSC sensitizers have been found to be beneficial for lowering the excited-state oxidation potential, thereby facilitating efficient injection of the electron into

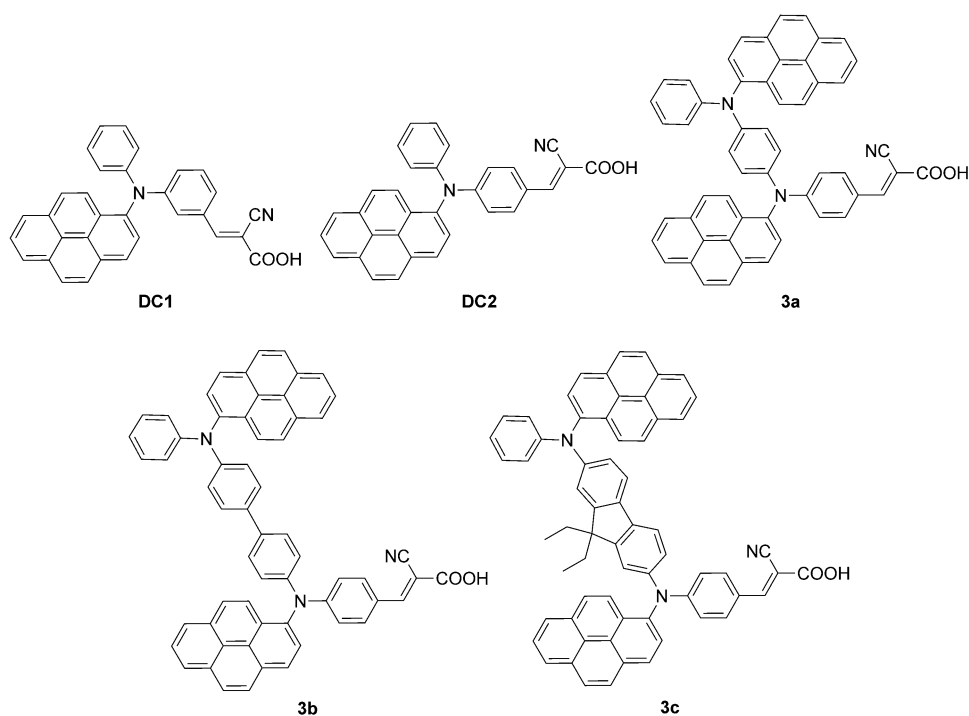
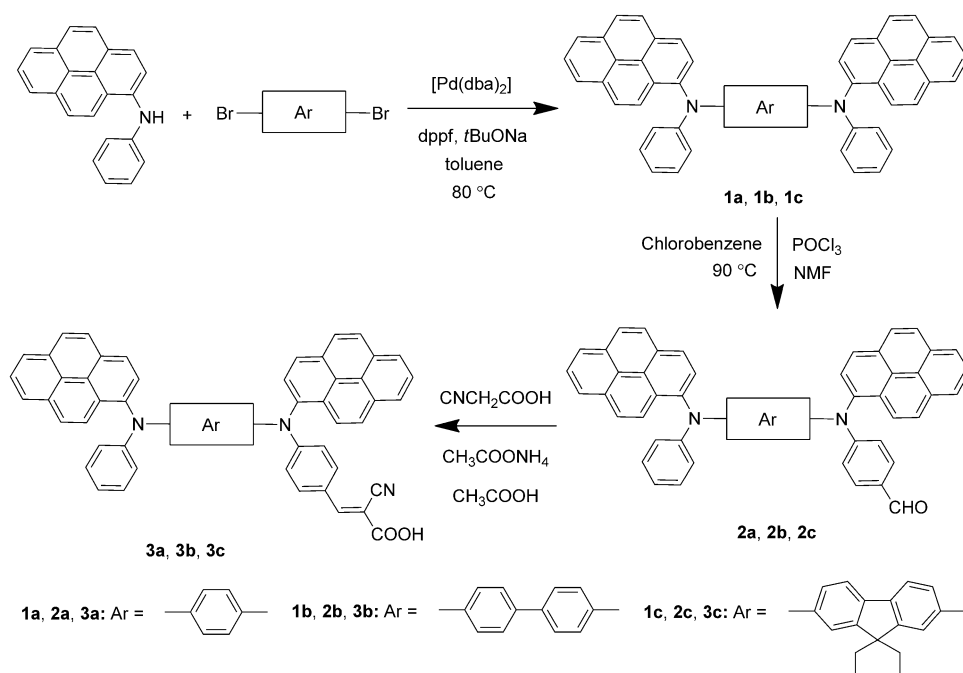


Figure 1. Structures of the dyes.

the conduction band of TiO₂. The conjugation pathway of the aromatic linker between the donors in the diamine system has been modified from biphenyl to fluorene as the nonplanar and planar linkers, respectively, are expected to differ in mediating electronic communication between the two donors and fine tune the ground- and excited-state properties of the dyes.^[5b] Though the organic sensitizers based on a cascade donor system^[10a,24,25] have been explored before for applications in DSSCs, the effect of the aromatic linker between the donors has not been studied in detail. We felt that fine tuning of the donor–donor interaction by altering the conjugation pathway can be used as a strategy to modulate the excited-state properties of the dyes and the stability of the cation radical produced after the electron ejection. Herein, we report the synthesis, characterization, optical properties, electrochemical characteristics, and DSSC studies of the newly developed dyes, which expose the importance of the π linker between the donors.

Results and DiscussionSynthesis

The dyes, **3a–3c**, were synthesized as illustrated in Scheme 1. The diamines (**1a–1c**) required for the present study were formed by a palladium-catalyzed C–N coupling reaction^[26] of the *N*-phenylpyrenyl-1-amine with the corresponding dibromoarene. They were then converted into the required aldehydes (**2a–2c**) by performing a Vilsmeier–Haack formylation using POCl₃ and *N*-methylformamide in chlorobenzene. The monoformylation selectively occurred at the *para* position of the phenyl unit rather than the pyrene

Scheme 1. Synthesis of the dyes **3a–3c**.

unit, and this paved the way for the subsequent preparation of the target dyes (**3a–3c**) by Knoevenagel condensation with cyanoacetic acid in the presence of ammonium acetate as the catalyst. The dyes **DC1** and **DC2** have also been synthesized as model compounds to study the impact of the conjugation and auxiliary donor on optical and electrochemical properties from the readily available aldehydes. The dyes are red in color and moderately soluble in solvents such as toluene, dichloromethane, tetrahydrofuran (THF), acetonitrile (MeCN), *N,N*-dimethylformamide (DMF), dimethyl sulfoxide (DMSO), and methanol to produce dark yellow solutions.

Optical Properties

The absorption spectra of dyes (**3a–3c**, **DC1**, and **DC2**), the precursor amines, and aldehydes were examined in dichloromethane (Figure 2) and the pertinent data are collected in Table 1. All the dyes exhibited three prominent absorption bands and invariably all the bands feature a shoulder at shorter wavelength, indicative of mixing of transitions. The higher energy band occurring at 275 nm is observed for all dyes and can be assigned to a pyrenylphenylamine localized $\pi-\pi^*$ transition.^[20,23] The incremental increase in the molar extinction coefficient for this band in the dyes **3a–3c**, when compared to the control dyes (**DC1** and **DC2**) is attributable to the presence of two pyrenylphenylamine units in the former dyes. The origin of the higher wavelength peaks appearing at approximately 320 and 430 nm are easily understood by comparing the absorption spectra of **DC1** with **DC2**. In **DC1**, the *meta* disposition of the cyanoacrylic acid

unit is not favorable for the intramolecular charge transfer from the amine to the cyanoacrylic acid unit. Thus, the peaks appearing for **DC1** at 305 and 375 nm are assigned to pyrene localized $\pi-\pi^*$ and amine-to-pyrene charge-transfer transitions, respectively.^[23] The absence of the later peak in the naphthalene analog *N,N'*-bis-(1-naphthyl)-*N,N'*-diphenyl-1,1'-biphenyl-4,4'-diamine (**NPB**)^[27] clearly validates the above assignment. The amine-to-pyrene charge-transfer transition exhibits an interesting trend, which is dependent on the donor strength of the amine. A slight blue-shift is observed for the compounds containing electron-withdrawing groups such as aldehyde 4-(phenyl(pyren-1-yl)amino)benzaldehyde (**PPAB**, **2a–2c**; see

below) when compared to that of parent amines. It is likely that the charge density on the amine unit is competitively withdrawn by both pyrene and aldehyde units. This would lead to the reduction in the strength of the donor–acceptor interaction between the amine and pyrene/aldehyde. Thus, the position of this peak is highly dependent on the donor strength of the amine; as the donor strength increases, the charge-transfer interaction with pyrene also increases (Table 1). The later peak is probably buried in the intense charge-transfer transition occurring in the dyes **DC2** and **3a–3c** at the higher wavelength region (> 400 nm).

The dye **DC2** shows the most red-shifted absorption in the series, while dye **3c** exhibits absorption with a high-

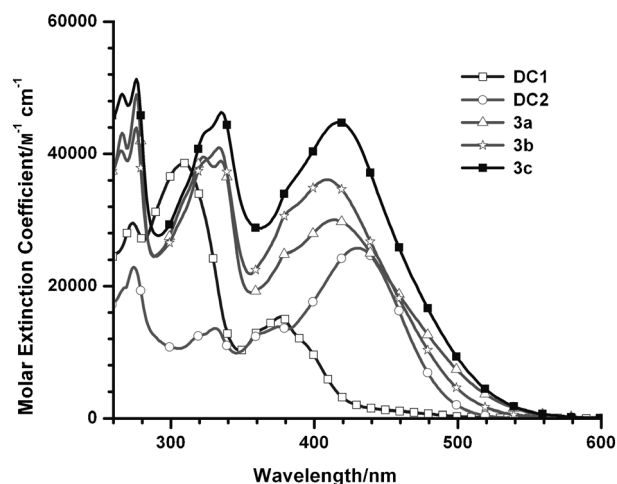


Figure 2. Absorption spectra of the dyes recorded in dichloromethane.

Table 1. Photophysical and electrochemical data of the compounds recorded for a dichloromethane solution.

| Dye ^[a] | λ_{max} [nm] (ϵ_{max} , $\text{M}^{-1}\text{cm}^{-1} \times 10^3$) | λ_{em} [nm] | Stokes shift [cm^{-1}] | E_{ox} (ΔE_p) [mV] ^[a] | HOMO [eV] | LUMO [eV] | E_{0-0} [eV] | E_{ox}^* [eV] |
|--------------------|---|----------------------------|-----------------------------------|--|-----------|-----------|----------------|------------------------|
| DPAP | 300 (25.7), 381 (14.1) | 469 | 4925 | 444 (69), 940 | 5.24 | 2.36 | 2.88 | – |
| 1a | 323 (55.5), 335 (54.2), 413 (22.5) | 562 | 6419 | 96 (48), 588 (64), 1128 | 4.90 | 2.25 | 2.65 | – |
| 1b | 334 (76.3), 406 (37.0) | 503 | 4750 | 280 (64), 532 (70), 992 | 5.08 | 2.28 | 2.80 | – |
| 1c | 337 (47.7), 362 (37.8), 418 (30.4) | 542 | 5473 | 140 (66), 492 (67), 1040 | 4.94 | 2.28 | 2.66 | – |
| PPAB | 329 (27.0), 349 (26.9), 378 (23.5) | 467 | 5042 | 604 (76), 976 | 5.40 | 2.45 | 2.95 | – |
| 2a | 336 (49.8), 381 (33.7) | 559 | 8358 | 236 (65), 644 (71), 1124 | 5.04 | 2.28 | 2.76 | – |
| 2b | 332 (50.7), 376 (47.7) | 497 | 6475 | 380 (63), 604 (69), 992 | 5.18 | 2.36 | 2.82 | – |
| 2c | 335 (50.2), 390 (52.2) | 513 | 6148 | 260 (76), 556 (80), 964 | 5.06 | 2.33 | 2.73 | – |
| DC1 | 274 (29.5), 309 (38.6), 377 (15.4) | 461 | 4833 | 544 (62), 972 | 5.34 | 2.40 | 2.94 | –1.626 |
| DC2 | 274 (22.9), 331 (13.6), 376 (13.8), 431 (25.7) | 484 | 2541 | 612 (65), 968 | 5.41 | 2.71 | 2.70 | –1.318 |
| 3a | 276 (49.0), 323 (39.5), 335 (38.9), 414 (30.0) | 561 | 6329 | 244 (48), 636 (48), 1108 | 5.04 | 2.51 | 2.53 | –1.516 |
| 3b | 276 (44.0), 334 (40.9), 409 (36.1) | 510 | 4664 | 392 (44), 608 (64), 1004 | 5.19 | 2.52 | 2.67 | –1.508 |
| 3c | 276 (51.3), 335 (46.3), 417 (44.8) | 545 | 5632 | 276 (47), 556 (64), 1060 | 5.07 | 2.51 | 2.56 | –1.518 |

[a] from cyclic voltammetry using scan rate 100 mV sec^{-1} and referenced to a ferrocene redox couple.

molar extinction coefficient. On introduction of the second amino unit, the peak position shifted slightly to the higher energy side for **3a–3c**. However, this cannot be treated as a blue-shift as the band showed significant broadening, indicative of the fusion of multiple peaks. Interestingly, the molar extinction coefficient of the higher wavelength peak progressively increased on the extension of the conjugation bridge connecting the two donor units. The rise in the optical density for the higher wavelength absorption for the dyes **3a–3c** may originate due to the following facts: a) a two-fold increase in the chromophoric density for the amine-to-pyrene charge-transfer electronic transition and b) the extension of the linker conjugation and its planarity, which may enhance the donor strength of the cascade donor system and increase the transition probability of the amine-to-cyanoacetic acid charge transfer. A slight blue-shift observed for the biphenyl-bridged derivative (**3b**), when compared to the phenyl-bridged (**3a**) and fluorene-bridged (**3c**) derivatives, suggests the presence of an inefficient interaction between the auxiliary amine donor and the pivotal amine donor, owing to noncoplanarity in the biphenyl bridge.

It is interesting to compare the absorption spectra of the dyes with the precursor amines and aldehydes (see Figures S4 and S5 in the Supporting Information) as they reveal the origin of certain transitions and are useful to understand the impact of the electron-accepting group. Firstly, the absorption peaks of amines **1a–1c** and aldehydes **2a–2c** are red-shifted when compared to that of the control amine, *N,N*-diphenylpyren-1-amine (**DPAP**) and the aldehyde, 4-(phenyl(pyren-1-yl)amino)benzaldehyde (**PPAB**), respectively. This red-shift originates because of the auxochromic

effect exerted by the additional amino segment linked through an aromatic unit such as phenyl, biphenyl, or fluorene. Secondly, the optical density of the dye precursors **1a–1c** and **2a–2c** are significantly larger than those of the control precursors **DPAP** and **PPAB**, respectively. This suggests that multiple transitions arising from different chromophore-localized electronic excitations overlap in the shorter wavelength region, thus resulting in the increase in molar extinction coefficient. Thirdly, the longer wavelength absorption grows in intensity on moving from amines (**1a–1c**) to aldehydes (**2a–2c**) with a concomitant blue-shift in the peak positions. This suggests that on introduction of an aldehyde functionality, an additional electronic transition corresponding to the amine-to-aldehyde charge-transfer appears; however, it merges with the transition attributable to the amine-to-pyrene charge-transfer from the higher energy side.

To understand the effect of environments on the electronic properties of the dyes, we have studied the absorption spectra of the dyes in solvents such as toluene, THF, dichloromethane, acetonitrile, and methanol with different polarity indices (Table 2). The changes in the absorption profiles for the dyes with solvent polarity are illustrated in Figure 3 for the dyes **DC2** and **3a**. In general, all the dyes exhibited red-shifted absorption in nonpolar solvents such as toluene and shorter wavelength absorption in the polar solvents such as methanol. The solvatochromism was most pronounced for **DC2** compared to that of dyes **3a–3c**. The dielectric constant of the solvents increases in the order of toluene < tetrahydrofuran < dichloromethane < methanol < acetonitrile. Considering the progressive increase in the effective solvation of the dye with solvent polarity, more red-

Table 2. Absorption properties of dyes in different solvent environments.

| Dyes | λ_{max} , nm (ϵ_{max} , $\text{M}^{-1} \text{cm}^{-1} \times 10^3$) | | | | | | | | |
|------------|--|--|--|-------------------------------------|------------------------------------|------------------------------------|------------------------------|------------------------------|------------------------------|
| | DCM | DCM+TFA | DCM+TEA | MeOH | MeOH+TFA | MeOH+NaOH | TOL | THF | MeCN |
| DC1 | 274 (29.5), 309 (38.6), 377 (15.4) | 273 (30.3), 311 (42.4), 376 (17.1) | 296 (35.6), 377 (15.2) | 272 (36.9), 296 (40.5), 376 (16.0) | 273 (32.4), 303 (40.6), 376 (16.9) | 272 (35.2), 296 (38.9), 376 (15.6) | 309, 379 ^[a] | 300, 377 ^[a] | 300, 376 ^[a] |
| DC2 | 274 (22.9), 331 (13.6), 376 (13.8), 431 (25.7) | 274 (23.9), 327 (13.6), 360 (12.9), 448 (31.4) | 332 (16.1), 402 (23.2) | 272 (31.9), 329 (22.2), 405 (36.9) | 271 (32.5), 329 (19.3), 423 (41.3) | 272 (25.5), 329 (18.1), 403 (29.6) | 332, 375, 431 ^[a] | 332, 376, 411 ^[a] | 330, 374, 420 ^[a] |
| 3a | 276 (49.0), 323 (39.5), 335 (38.9), 414 (30.0) | 276 (58.6), 322 (43.9), 333 (43.9), 381 (29.5), 408 (30.9), 460 (28.1) | 276 (48.9), 322 (39.9), 336 (39.9), 410 (33.9) | 274 (31.9), 333, 407 ^[a] | 274, 319, 332, 412 ^[a] | 274, 319, 333, 406 ^[a] | 324, 337, 415 ^[a] | 322, 335, 413 ^[a] | 320, 333, 406 ^[a] |
| 3b | 276 (44.0), 334 (40.9), 409 (36.1) | 275 (51.3), 331 (47.0), 378 (32.3), 401 (29.6), 460 (36.3) | 276 (44.0), 335 (42.4), 405 (42.8) | 273, 331, 403 ^[a] | 273, 330, 411 ^[a] | 273, 331, 403 ^[a] | 334, 411 ^[a] | 333, 410 ^[a] | 332, 400 ^[a] |
| 3c | 276 (51.3), 335 (46.3), 417 (44.8) | 276 (54.6), 334 (48.2), 380 (36.2), 416 (40.9), 463 (33.2) | 322 (38.8), 336 (38.7), 409 (32.8) | 274, 333, 410 ^[a] | 274, 332, 412 ^[a] | 274, 333, 410 ^[a] | 337, 419 ^[a] | 335, 415 ^[a] | 336, 420 ^[a] |

[a] Molar extinction coefficients could not be obtained due to poor solubility.

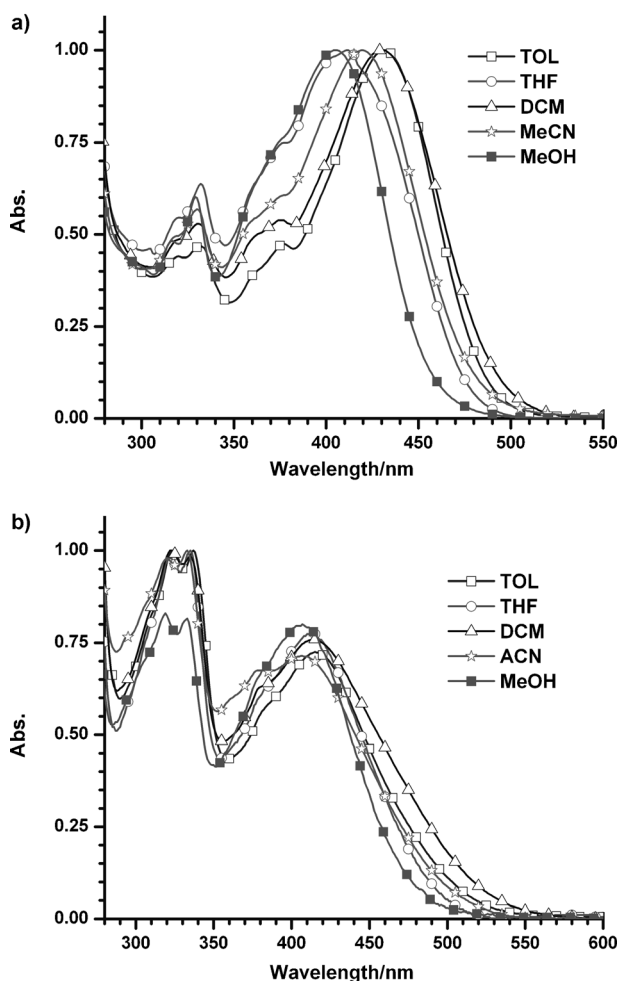


Figure 3. Absorption spectra recorded for a) **DC2** and b) **3a** in different solvents.

shifted absorption in toluene and shorter wavelength absorption in acetonitrile were expected. However, the dye **DC2** showed significant blue-shifted absorption peaks in tetrahydrofuran and methanol. This is in agreement with the hydrogen-bonding parameters of the solvents (toluene < ace-

tonitrile < dichloromethane < tetrahydrofuran < methanol). It is probable that the hydrogen-bonding interaction of the solvents such as tetrahydrofuran and methanol with the dye might alter the acceptor ability of the carboxylic acid unit, analogous to the interaction of the dye with the TiO₂ surface. To further confirm the interaction of the dye with methanol, absorption spectra of the dye **DC2** in acetonitrile with different amounts of methanol were recorded (Figure 4). A significant blue-shift was noticed on increasing the methanol concentration; this is consistent with the above proposition.

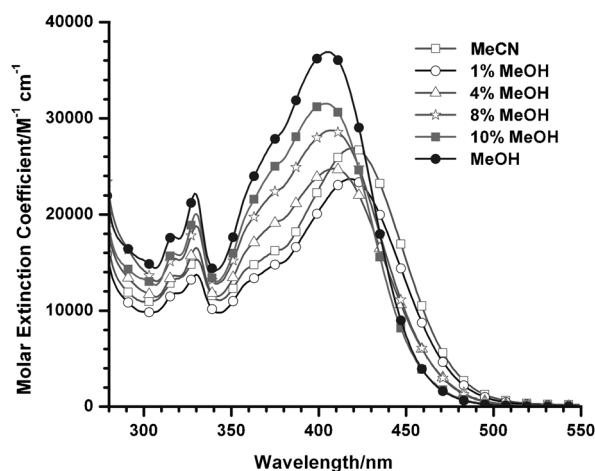


Figure 4. Absorption spectra of **DC2** recorded in acetonitrile and methanol mixtures.

The dyes have also shown changes in the absorption upon addition of trifluoroacetic acid (TFA) and triethylamine (TEA) to the dichloromethane and methanol solutions, indicative of the presence of acid–base equilibria (Figure 5). The dyes exhibited a red-shift upon addition of TFA to the dichloromethane solution, while addition of TEA to the solution resulted in a blue-shift. Such behavior has been noticed for several organic dyes, developed for DSSC applications, which contain a cyanoacrylic acid acceptor unit.^[17]

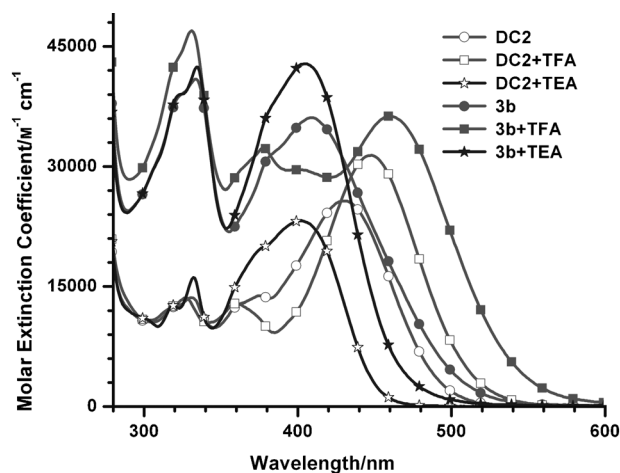


Figure 5. Changes in the absorption spectra of the dyes **DC2** and **3b** in dichloromethane upon addition of TFA or TEA.

Similarly, addition of TFA to the methanolic solution of the dyes also led to a prominent red-shift but the addition of sodium hydroxide or TEA did not alter the absorption peak (see the Supporting Information). This suggests the presence of the deprotonated form for the dyes in the methanol solution.

The emission spectra of the dyes were recorded in dichloromethane and are displayed in Figure 6. The shortest wavelength emission peak was observed for **DC1** while the longest wavelength emission was found for **3a**. While the absorption wavelengths are similar for the dyes **3a–3c**, the significant difference observed in the emission peaks (**3a** > **3c** > **3b**) is surprising. It appears that the nature of the aromatic segment that bridges the auxiliary donor with the main donor plays a major effect in the excited state. In **3a**, through the shorter phenylene linkage, the auxiliary donor enhances the donor strength of the main donor, while in **3b** the twisted biphenyl bridge decouples the auxiliary donor from the main donor. Thus in **3a**, the electronic excitation, which arises due to the charge transfer from the amine to

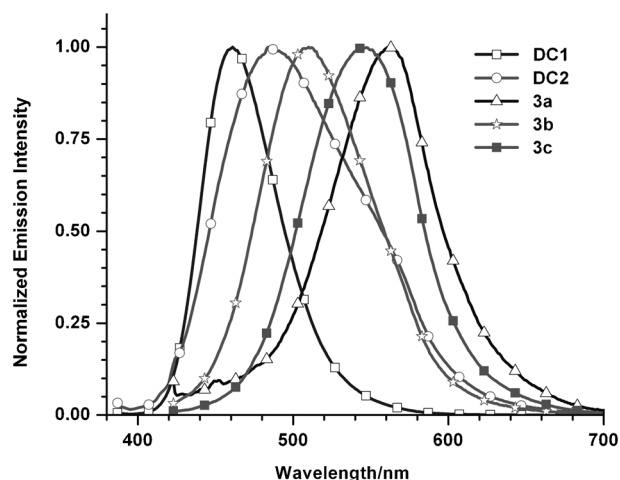


Figure 6. Emission spectra of the dyes recorded in dichloromethane.

the cyanoacrylic acid acceptor would cause a migration of electron density from the auxiliary donor toward the acceptor, while this would be less pronounced in **3b**. The net result is a more polar excited state for **3a**, which would facilitate a dipolar relaxation with the solvent dipoles when compared to the dye **3b**. The higher wavelength shoulder observed in the emission spectra of **DC2** was speculated to originate from the excimer. This assignment was confirmed by analyzing the concentration dependence of the emission profile. At higher concentrations the shoulder observed at 550 nm has grown in intensity and appeared as a prominent peak (Figure 7). It is interesting to note that such excimer

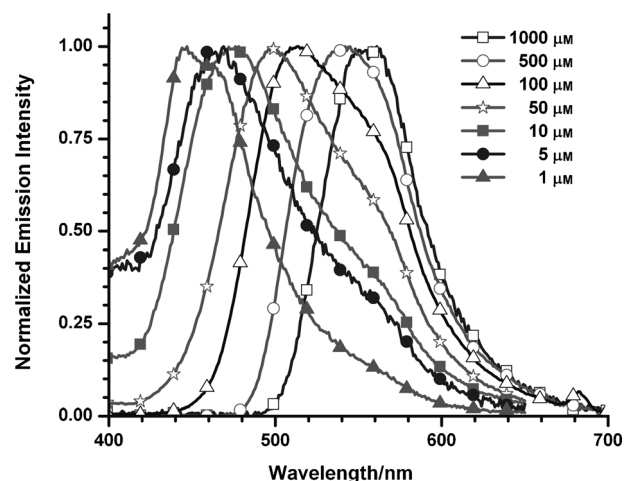


Figure 7. Emission spectra of **DC2** recorded for dichloromethane solutions of different concentrations.

formation owing to the intermolecular interaction of pyrene units was prohibited in the dyes **3a–3c** due to the introduction of an auxiliary triarylamine segment, which effectively inhibits the approach of two pyrene units. It is likely that the dyes, **3a–3c**, are prone to resist aggregation at the surface of the TiO_2 due to the nonplanar structural elements, and this property will be beneficial for the photocurrent generation.

Electrochemical Properties

The dyes were analyzed by cyclic voltammetric experiments to understand the redox propensity of the dyes. In order for the dyes to effectively function as a sensitizer in DSSCs, they must possess ground-state oxidation potentials lower than that of the electrolyte and the first excited-state oxidation potential above the conduction band of TiO_2 .^[4] The dyes fulfilling the above criteria will effectively inject electrons into the conduction band of TiO_2 from the excited state and will allow regeneration of the dye by the electrolyte. The cyclic voltammetric measurements were performed in dichloromethane solutions (2×10^{-4} M) using tetrabutylammonium hexafluorophosphate as a supporting electrolyte.

The cyclic voltammograms recorded for the dyes **DC2**, **3b**, and **3c** along with their amine precursors (**DPAP**, **1b**, and **1c**) in the presence of ferrocene are shown in Figure 8 and the relevant data are collected in Table 1. The dyes **DC1** and **DC2** exhibited a quasi-reversible oxidation couple at

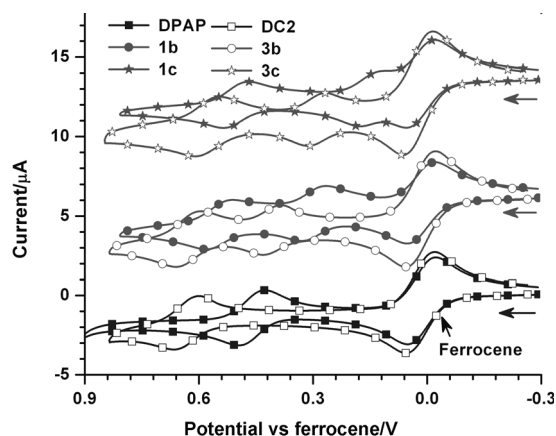


Figure 8. Cyclic voltammograms recorded in dichloromethane at the scan rate 100 mV/sec using ferrocene as an internal standard for the dyes **DC2**, **3b**, and **3c**. The cyclic voltammograms of their parent amines **DPAP**, **1b**, and **1c** (solid lines) are also shown for comparison.

higher positive potentials than that of ferrocene, which is attributable to the oxidation of the triarylamine segment. The diamine-based dyes **3a–3c** displayed two quasi-reversible oxidation couples, which arise from the two different amino groups. The redox couple located at the lower oxidation potential is assigned to the triarylamine segment that is further away from the cyanoacrylic unit, while the oxidation occurring at the higher potential is attributed to the triarylamine segment bearing the cyanoacrylic acid unit, which will be difficult to oxidize. Facile first oxidation observed for the dyes **3a** and **3c** when compared to **3b** is suggestive of a stronger electronic interaction between the donor segments through the short phenylene unit in **3a** and planar fluorene segment in **3c**. Whereas in **3b**, the twisted biphenyl unit is probably inhibiting the electronic interaction between the donor units. The highest second oxidation potential observed for **3a** in the series is corroborative of the above arguments. The oxidation potentials of the dyes are more positive when compared to the corresponding values of the parent amines (**DPAP**, **1a–1c**), and this confirms the presence of intramolecular charge-transfer interactions between donor and acceptor units and within the cascade donor segment.^[24] This also points out that the interaction between the donors in the cascade donor system is affected by the nature of the bridging unit.

To identify the feasibility of dye regeneration by the iodine/iodide electrolyte system, we have measured the ground-state oxidation potentials of the dyes (see Table 1), which fall in the range 1.31–1.38 V versus the normal hydrogen electrode (NHE) for the control dyes (**DC1** and **DC2**), however, the dyes **3a–3c** exhibited lower values (1.01–

1.16 V vs. NHE). The values are more positive than the iodide/triiodide redox couple (ca. 0.42 V vs NHE). This ensures the efficient regeneration of the dye from the oxidized dye by the receipt of an electron from the electrolyte. The redox potentials of dyes **3a–3c** match well with that of the electrolyte, as compared to the dyes **DC1** and **DC2**, owing to the presence of two triarylamine donor segments in the former dyes, which enhance the donor strength and substantially lower the highest occupied molecular orbital (HOMO) energy levels of the dyes (**3a–3c**).

We have also estimated the excited-state oxidation potentials (E_{ox}^*) of the sensitizers, which correspond to the LUMO levels of the dyes, to estimate the thermodynamic driving force for the injection of electrons from the dye into the conduction band of TiO_2 . The excited-state potential was calculated from the first oxidation potential (E_{ox}) at the ground-state and the zero-zero electronic transition energy (E_{0-0}) from $E_{ox}^* = E_{ox} - E_{0-0}$. The optical band gap was derived from the absorption edge. A dye must possess a more negative excited-state potential than the energy level of the TiO_2 conduction band edge (−0.5 V vs NHE) for energetically favorable downhill electron injection.^[24] The E_{ox}^* values observed for the dyes (−1.32 to −1.63 V vs NHE) are more negative than the conduction-band-edge energy level of the TiO_2 electrode. Thus, these dyes are expected to effectively inject electrons into the TiO_2 conduction band.

Theoretical Investigations

Density functional theory (DFT) calculations^[28] have been employed to optimize the geometry of the compounds and rationalize the origin of the absorption spectra observed for these dyes (**DC1**, **DC2**, and **3a–3c**). The prominent higher wavelength vertical transitions, their oscillator strengths (f), and dipole moments obtained from the computations are collected in Table 3.

Electronic distributions in the frontier molecular orbitals of the dyes, **3a–3c**, are displayed in Figure 9 while the corresponding results for the control dyes are shown in Figure S15 in the Supporting Information. In **DC1**, HOMO and HOMO-1 are mainly contributed by the pyrenylphenylamine segment, whereas in **DC2** they are delocalized over the entire molecule. The LUMO is located on the cyanoacrylic unit and is extended up to the phenyl ring, while the LUMO+1 is constituted primarily by the pyrene unit in **DC1** and **DC2**. The longer wavelength vertical transition of **DC2** is mainly due to the electronic excitation from the HOMO to LUMO, while in **DC1** it arises due to electronic promotion from the HOMO to LUMO+1 with little contribution from HOMO-1 to LUMO and LUMO+1. This clearly suggests that in **DC1** the prominent excitation leads to the charge transfer from the amine to pyrene segments, while in **DC2** the charge transfer occurs from the amine to cyanoacrylic acid. The shorter wavelength vertical transition observed for **DC1** when compared to **DC2** is also consistent with the experimental observation (see above).

Table 3. Predicted (TDDFT B3LYP/6-31G(d,p)) vertical transitions and their assignments.

| Dye | λ_{abs} [nm] | f | μ , [Debye] | Assignment |
|------------|-----------------------------|------|-----------------|---|
| DC1 | 408.6 | 0.26 | 7.33 | HOMO→LUMO+1 (+77%), HOMO-1→LUMO (13%), HOMO-1→LUMO+1 (+8%) |
| | 326.4 | 0.17 | | HOMO-1→LUMO+1 (+73%), HOMO-2→LUMO+1 (6%), HOMO→LUMO+1 (6%), HOMO-2→LUMO+2 (+6%), HOMO→LUMO+2 (5%) |
| | 310.0 | 0.19 | | HOMO→LUMO+3 (+62%), HOMO-2→LUMO+1 (11%), HOMO→LUMO+2 (+9%), HOMO-1→LUMO+2 (+9%) |
| | 305.5 | 0.36 | | HOMO-3→LUMO (54%), HOMO-4→LUMO (41%) |
| DC2 | 440.2 | 0.43 | 8.19 | HOMO→LUMO (+95%) |
| | 407.0 | 0.11 | | HOMO→LUMO+1 (+78%), HOMO-1→LUMO (13%), HOMO-1→LUMO+1 (+7%) |
| | 368.1 | 0.48 | | HOMO-1→LUMO (+81%), HOMO-1→LUMO+1 (+7%), HOMO→LUMO+1 (+7%) |
| | 333.3 | 0.21 | | HOMO-1→LUMO+1 (+72%), HOMO→LUMO+1 (8%), HOMO-2→LUMO+2 (6%) |
| 3a | 489.1 | 0.40 | 9.58 | HOMO→LUMO (+98%) |
| | 451.2 | 0.31 | | HOMO→LUMO+1 (+92%) |
| | 420.3 | 0.12 | | HOMO-1→LUMO (+94%), HOMO-2→LUMO (5%) |
| | 382.4 | 0.15 | | HOMO-1→LUMO+1 (56%), HOMO-2→LUMO (+32%) |
| | 369.4 | 0.12 | | HOMO-2→LUMO (59%), HOMO-1→LUMO+1 (24%) |
| | 351.0 | 0.23 | | HOMO-3→LUMO (+48%), HOMO→LUMO+4 (18%), HOMO-2→LUMO+1 (10%), HOMO→LUMO+3 (+10%) |
| | 348.2 | 0.26 | | HOMO-3→LUMO (+35%), HOMO→LUMO+3 (26%) |
| | | | | HOMO→LUMO (+98%) |
| 3b | 487.1 | 0.31 | 9.59 | HOMO→LUMO (+98%) |
| | 446.5 | 0.41 | | HOMO→LUMO+1 (+71%), HOMO→LUMO+2 (+21%), |
| | 434.8 | 0.41 | | HOMO-1→LUMO (+68%), HOMO→LUMO+2 (+20%) |
| | 378.7 | 0.29 | | HOMO-2→LUMO (+73%), HOMO-3→LUMO (11%), HOMO-1→LUMO+1 (+7%) |
| | 362.8 | 0.38 | | HOMO-1→LUMO+2 (+43%), HOMO-3→LUMO (+35%), HOMO-2→LUMO (+9%) |
| | 347.9 | 0.35 | | HOMO→LUMO+3 (+51%), HOMO-2→LUMO+1 (14%) |
| 3c | 516.3 | 0.21 | 8.31 | HOMO→LUMO (+99%) |
| | 468.6 | 0.48 | | HOMO→LUMO+1 (+88%), HOMO→LUMO+2 (+7%) |
| | 444.2 | 0.28 | | HOMO→LUMO+2 (+75%), HOMO-1→LUMO (+14%) |
| | 435.6 | 0.24 | | HOMO-1→LUMO (+81%), HOMO→LUMO+2 (+12%) |
| | 368.9 | 0.51 | | HOMO-3→LUMO (+58%), HOMO→LUMO+4 (+26%), HOMO-2→LUMO (+8%) |
| | 362.4 | 0.11 | | HOMO-1→LUMO+2 (+82%), HOMO→LUMO+4 (7%), HOMO→LUMO+5 (+7%) |
| | 356.5 | 0.16 | | HOMO→LUMO+3 (+34%), HOMO→LUMO+4 (+24%), HOMO-2→LUMO+1 (+13%), HOMO-1→LUMO+3 (+11%), HOMO-3→LUMO (+6%) |

For the diamine-based dyes (**3a–3c**), the picture is entirely different. The HOMO is mainly distributed over the amine segment that is further away from the acceptor unit for **3b** and **3c**, while in **3a** it is spread up to the amine containing the acceptor unit. The LUMO in the dyes is mainly delocalized over the phenylcyanoacrylic acceptor unit and the LUMO+1 is composed of the pyrene segment. There are two prominent electronic excitations predicted for these dyes. The longer wavelength transition is due to the electronic excitation from the HOMO to LUMO, while the next absorption is from the HOMO to LUMO+1 electronic transition. This clearly indicates that in these dyes the longer wavelength transition is due to the charge transfer from the amine to cyanoacrylic acid acceptor, whereas the second transition stems from the charge transfer from the amine to the pyrene unit. On changing the conjugation pathway of the linker that separates the two amine units from phenyl to biphenyl or fluorene decreases the oscillator strength of the first absorption with a concomitant increment in the second absorption. It is interesting to note that extension of the conjugation between the amine units in this class of compounds is disadvantageous for the desired charge-transfer transition due to the competitive charge migration from the amine to the pyrene unit, with the latter being prominent for the dyes with an elongated conjugation pathway. The theoretically computed dipole moment is larger for the dia-

mine dyes (**3a–3c**) compared to that of control dyes (**DC1** and **DC2**), thus implying a strong dipolar interaction in the diamine dyes due to the presence of a cascade donor system.

Photovoltaic Device Performance

The DSSCs were constructed by using the dyes (**DC1**, **DC2**, and **3a–3c**) as the sensitizer for nanocrystalline anatase TiO₂. Typical solar cells, with an effective area of 0.25 cm², were fabricated with an electrolyte composed of 0.05 M I₂/0.5 M LiI/0.5 M *tert*-butylpyridine in acetonitrile solution. The device performance statistics were obtained under AM 1.5 solar irradiation and collected in Table 4. The current–voltage curves of the DSSCs sensitized by the dyes are shown in Figure 10.

Among the control dyes, **DC2** shows better efficiency due to the donor–acceptor structure, whereas in **DC1** the cyanoacrylic acid is delinked from the donor by *meta* disposition. The DSSCs sensitized by the dyes **3a** and **3c** have exhibited the higher η values 4.28% ($J_{\text{sc}}=10.2 \text{ mA cm}^{-2}$, $V_{\text{oc}}=0.595 \text{ V}$, $ff=0.71$) and 3.89% ($J_{\text{sc}}=9.51 \text{ mA cm}^{-2}$, $V_{\text{oc}}=0.583 \text{ V}$, $ff=0.70$), respectively. The dyes featuring diamines (**3a–3c**) show higher current conversion efficiency than the control dyes **DC1** and **DC2**, which is attributed to the larger

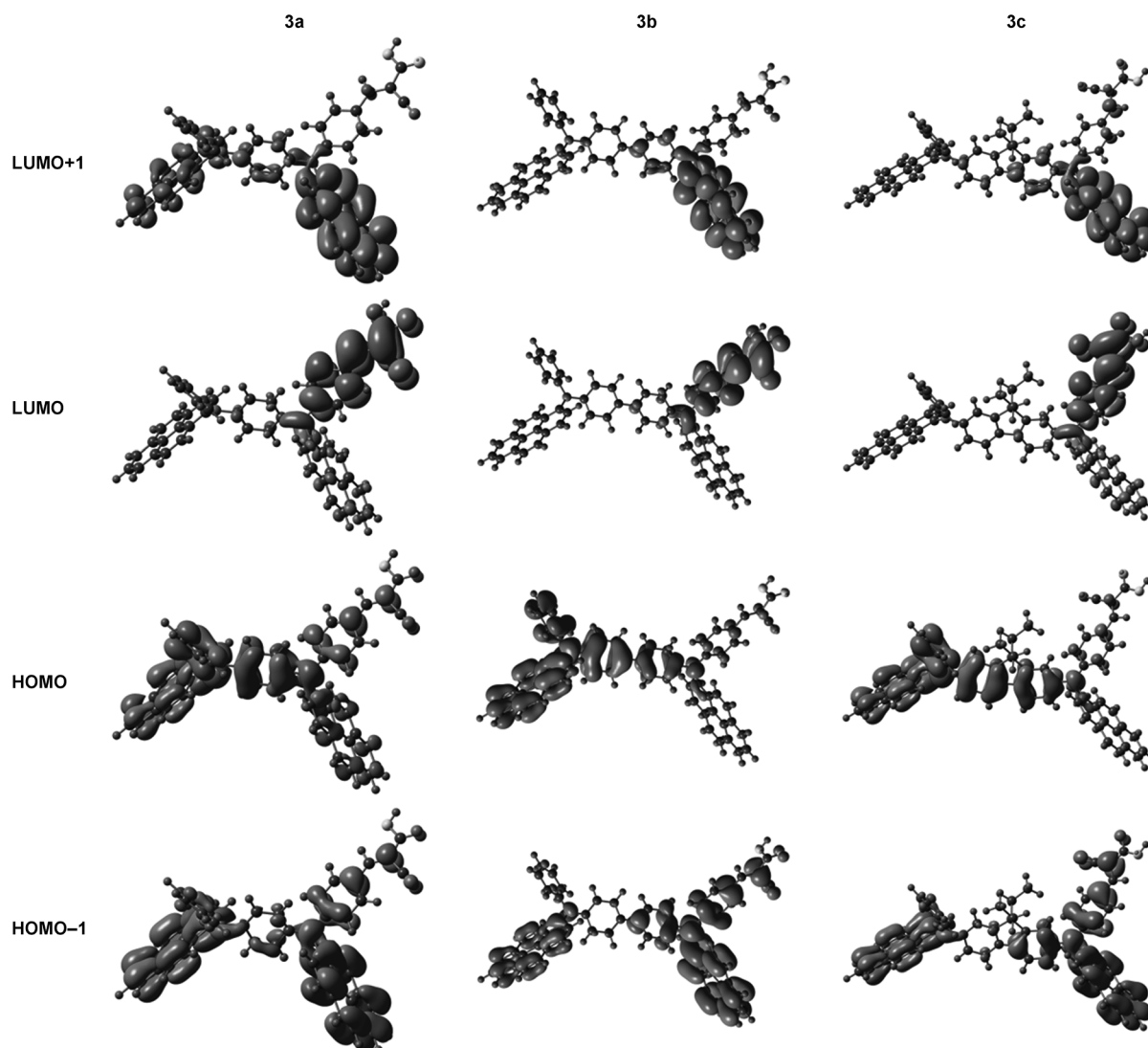


Figure 9. Electronic distribution observed for the frontier orbitals for the dyes **3a-3c**.

Table 4. Performance characteristics of the DSSCs fabricated using the dyes.

| Dyes | J_{sc} [mA cm^{-2}] | V_{oc} [mV] | ff | η [%] | R_{ct2} [ohm] | f_{max} | τ_e [ms] |
|------------|----------------------------------|---------------|------|------------|----------------------------|-----------|---------------|
| DC1 | 2.48 | 472 | 0.43 | 0.51 | 86.36 | 34.36 | 4.63 |
| DC2 | 6.27 | 516 | 0.71 | 2.29 | 19.84 | 112.98 | 1.41 |
| 3a | 7.20 | 577 | 0.69 | 2.88 | 27.93 | 92.68 | 1.72 |
| 3b | 10.2 | 595 | 0.71 | 4.28 | 17.50 | 7.01 | 22.69 |
| 3c | 9.51 | 583 | 0.70 | 3.89 | 17.24 | 8.55 | 18.61 |

molar extinction coefficient for the charge-transfer transition in the former dyes, and this is a result of the cascade donor system. In fact the enhancement of donor strength owing to the presence of the cascade donor system in **3a-3c** is manifested in the incident photo-to-current conversion efficiency (IPCE) spectra (Figure 11). The dyes **3a-3c** showed higher power conversion efficiencies at longer wavelength

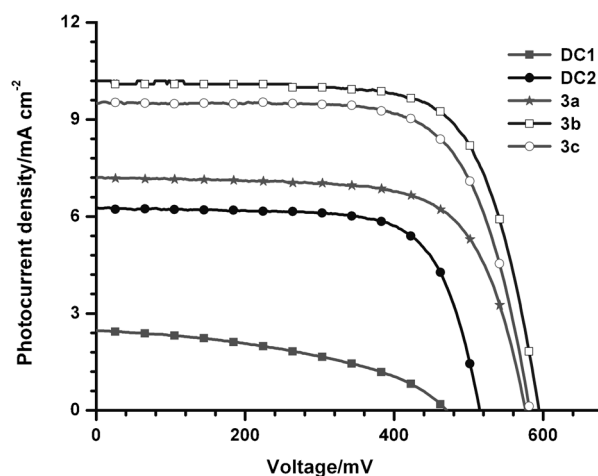


Figure 10. The current-voltage (I - V) characteristics of the DSSCs fabricated using the dyes.

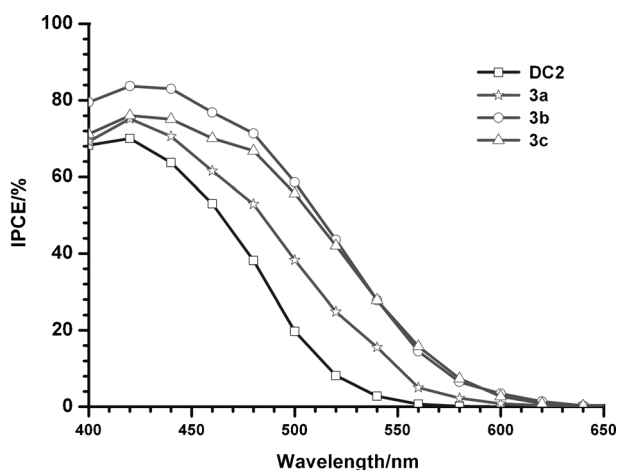


Figure 11. IPCE spectra recorded for the DSSCs fabricated using the dyes, **DC2**, **3a–3c**.

incident light when compared to the control dye **DC2**. This suggests that the light harvesting at the lower energy radiation is facilitated for the dyes **3a–3c** due to the presence of a stronger donor–acceptor interaction, a consequence of the cascade donor system. The highest device efficiency observed for **3b** in the series is attributed to the tilting in the biphenyl segment, which inhibits the intramolecular charge recombination, while for the planar segments phenyl and fluorene, the intramolecular charge recombination may be easier.

The Nyquist plot displayed in Figure 12a shows two semi-circles, which correspond to the charge-transfer resistances at the counter electrode and $\text{TiO}_2/\text{dye}/\text{electrolyte}$ interface, respectively. The radius of the bigger semicircle of the dye **3a** is significantly larger than the other dyes (**DC2**, **3b**, and **3c**), and this indicated the enlarged charge-transfer resistance for this dye. The charge-transfer resistance assumes the order of $3b < DC2 < 3c < 3a$. The V_{oc} for the devices increases in the order of $DC2 < 3a < 3c < 3b$. It is probable that the dyes based on cascade donors significantly alter the Fermi level of photoanode, which manifests in the V_{oc} . In the Bode-phase plot (Figure 12b), the prominent lower frequency peak of the dyes **3a** and **DC2** are shifted to higher frequency when compared to those of other dyes (**3b** and **3c**). This corresponds to a decrease in the electron lifetime for the **3a** and **DC2** sensitized DSSCs. The electron lifetime can be extracted from the angular frequency (ω_{min}) at the mid-frequency peak in the Bode-phase plot by using $\tau_e = 1/\omega_{min}$. The electron lifetime measured for the dyes **3a**, **3b**, and **3c** are 1.7, 22.7, and 18.6 ms, respectively, and follows the trend, $DC2 \approx 3a < 3c < 3b$. The increase in electron lifetime for **3b** supports more effective suppression of the back reaction of the injected electrons with the I_3^- in the electrolyte by alternation of the HOMO of the sensitizer, which leads to the improvement in the photocurrent and photovoltage and to the substantial enhancement of the device efficiency. Despite the enhancement in the electron lifetime, the lower device efficiency observed for the DSSC based on **3c** is at-

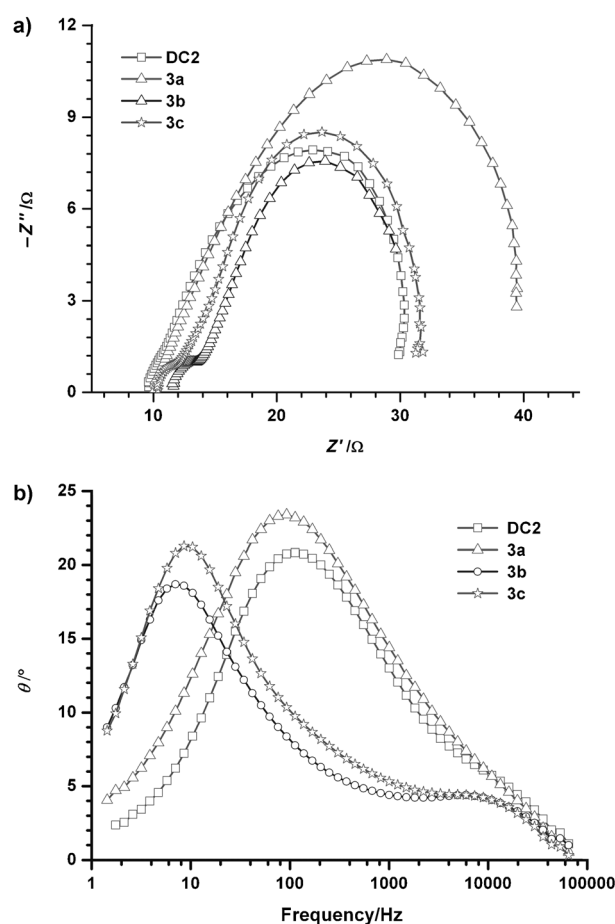


Figure 12. a) Nyquist and b) Bode-phase plots of the DSSCs fabricated using the dyes (**DC2**, **3a–3c**).

tributed to the lower number of photoinduced electron generation and the reduced electron injection efficiency of **3c**. The high-frequency peak observed in the Bode plot corresponds to charge transfer at the counter electrode. Slight changes observed for this peak indicate a probable reaction at the counter electrode/electrolyte interface.

Conclusions

In summary, we have synthesized new dyes containing 1-pyrenylphenylamino donors and cyanoacrylic acid acceptors. Dyes containing two cascade 1-pyrenylphenylamino donors have also been successfully synthesized and demonstrated as efficient sensitizers for DSSCs. The incorporation of an additional donor increases the absorption parameters such as molar extinction coefficient. Tuning of the optical and electrochemical properties has been achieved by the insertion of an aromatic segment of varied conjugation pathway length between the two donor units.

The oxidation potentials of the diamine-based dyes were higher than the monoamine-based control dyes, thereby illustrating the importance of cascade donor system to tune the HOMO of the dyes. Theoretical calculations revealed

the presence of two charge-transfer transitions from the amine to cyanoacrylic acid and pyrene units, respectively. The dye (**3b**) possessing a biphenyl linker between the donors exhibited higher photocurrent conversion efficiency $\eta = 4.28\%$. It appears that the retardation of intramolecular charge recombination at the excited state owing to the tilting in the biphenyl segment is beneficial for the light-harvesting properties.

Experimental Section

General details regarding the synthesis, characterization, physical measurements, theoretical computations, device fabrication, and characterization are similar to that reported in our earlier publication.^[10a]

Synthesis of N^1, N^4 -diphenyl- N^1, N^4 -di(pyren-1-yl)benzene-1,4-diamine (**1a**)

A mixture of 1,4-dibromopyrene (0.5 g, 2.1 mmol), *N*-phenylpyren-1-amine^[21b] (1.4 g, 4.7 mmol), [Pd(dba)₂] (dba = (1*E*,4*E*)-1,5-diphenylpenta-1,4-dien-3-one; 49 mg, 0.09 mmol), 1,1'-bis(diphenylphosphino)ferrocene (dppf; 47 mg, 0.09 mmol), sodium *tert*-butoxide (0.6 g, 6.4 mmol), and toluene (30 mL) was put in a pressure tube. It was heated at 80 °C and stirred for 48 h. After completion of the reaction, it was quenched by the addition of water and extracted with dichloromethane. The combined extracts were washed with a brine solution and dried over anhydrous Na₂SO₄. Rotary evaporation of the extracts gave the crude product, which was purified by silica-gel column chromatography using a mixture of hexanes/dichloromethane (1:4) to produce a yellow solid; yield 0.9 g (65%); m.p. 320–322 °C; ¹H NMR (CDCl₃, 500 MHz): $\delta = 8.17$ –8.16 (m, 6H), 8.12 (d, $J = 7.5$ Hz, 2H), 8.04 (s, 4H), 7.98 (t, $J = 7.8$ Hz, 3H), 7.95 (d, $J = 9.5$ Hz, 1H), 7.87–7.85 (m, 2H), 7.18–7.14 (m, 4H), 7.01–6.98 (m, 8H), 6.89–6.86 ppm (m, 2H); ¹³C NMR (CDCl₃, 125 MHz): $\delta = 143.0$, 131.1, 130.9, 129.2, 128.9, 127.6, 127.3, 127.0, 126.8, 126.1, 126.0, 125.8, 125.0, 124.8, 124.6, 123.7, 123.2, 120.7, 120.6 ppm.

Synthesis of N^4, N^4 -diphenyl- N^4, N^4 -di(pyren-1-yl)biphenyl-4,4'-diamine (**1b**)

Derivative **1b** was prepared by following a procedure similar to that described above for **1a**: yellow solid; yield 80%; m.p. 310–312 °C; ¹H NMR (CDCl₃, 500 MHz): $\delta = 8.17$ (d, $J = 8.5$ Hz, 5H), 8.14 (s, 1H), 8.11 (d, $J = 7.5$ Hz, 2H), 8.06 (s, 4H), 7.99–7.97 (m, 2H), 7.93 (d, $J = 8.0$ Hz, 2H), 7.86 (d, $J = 8.0$ Hz, 2H), 7.39–7.37 (m, 4H), 7.23–7.19 (m, 4H), 7.12–7.07 (m, 8H), 6.96 ppm (t, $J = 7.0$ Hz, 2H); ¹³C NMR (CDCl₃, 125 MHz): $\delta = 147.5$, 146.4, 139.7, 132.8, 130.2, 130.0, 128.7, 128.5, 128.2, 127.7, 127.6, 127.1, 126.9, 126.6, 126.2, 126.14, 126.08, 125.5, 125.3, 125.2, 125.0, 124.2, 124.1, 123.8, 122.3, 121.3, 121.2, 121.1, 120.8 ppm.

Synthesis of 9,9-diethyl- N^2, N^7 -diphenyl- N^2, N^7 -di(pyren-1-yl)-9*H*-fluorene-2,7-diamine (**1c**)

Derivative **1c** was prepared by following a procedure similar to that described above for **1a**: yellow solid; yield 74%; m.p. 250–253 °C; ¹H NMR (CDCl₃, 500 MHz): $\delta = 8.17$ –8.13 (m, 6H), 8.09 (d, $J = 7.5$ Hz, 2H), 8.05 (s, 4H), 8.00–7.97 (m, 2H), 7.89 (d, $J = 9.0$ Hz, 2H), 7.83 (d, $J = 8.5$ Hz, 2H), 7.39 (d, $J = 8.5$ Hz, 2H), 7.22–7.16 (m, 4H), 7.10 (d, $J = 2.0$ Hz, 2H), 7.07–7.05 (m, 4H), 6.96–6.94 (m, 4H), 1.69 (q, $J = 7.5$ Hz, 4H), 0.34 ppm (t, $J = 7.5$ Hz, 6H); ¹³C NMR (CDCl₃, 125 MHz): $\delta = 151.0$, 149.0, 147.3, 141.2, 135.8, 131.1, 130.9, 129.1, 129.0, 128.1, 127.6, 127.4, 127.1, 126.7, 126.2, 126.0, 125.8, 124.9, 124.8, 124.7, 123.4, 121.9, 121.6, 121.2, 119.5, 117.3, 55.9, 32.4, 8.3 ppm.

Synthesis of 4-((4-phenyl(pyren-1-yl)amino)phenyl)(pyren-1-yl)amino)benzaldehyde (**2a**)

N^1, N^4 -diphenyl- N^1, N^4 -di(pyren-1-yl)benzene-1,4-diamine (0.66 g, 1 mmol) was dissolved in chlorobenzene (20 mL) and *N*-methyl-*N*-phenylformamide (NMF; 0.2 mL, 1.5 mmol). Then, POCl₃ (0.14 mL, 1.5 mmol) was added dropwise at room temperature. The reaction mixture was stirred

and heated at 90 °C for 12 h. After completion of the reaction, as evidenced by the disappearance of aldehyde, the reaction mixture was poured into ice water and neutralized by sodium bicarbonate. The solution was extracted with dichloromethane, washed with brine solution, dried over Na₂SO₄, followed by evaporation of solvent. The desired product was purified by silica-gel column chromatography eluting with DCM/EtOAc mixture (1:9). The obtained product was further recrystallized with dichloromethane and methanol: yellow solid; yield 0.28 g (41%); m.p. 192–194 °C; IR (KBr): $\tilde{\nu}_{C=O} = 1686$ cm⁻¹; ¹H NMR (CDCl₃, 500 MHz): $\delta = 9.75$ (s, 1H), 8.23–8.21 (m, 2H), 8.18–8.16 (m, 3H), 8.14–8.12 (m, 2H), 8.10–8.08 (m, 3H), 8.05 (d, $J = 1.5$ Hz, 2H), 8.04–7.99 (m, 3H), 7.95 (d, $J = 9.5$ Hz, 1H), 7.90–7.85 (m, 2H), 7.63 (d, $J = 9.0$ Hz, 2H), 7.21–7.15 (m, 4H), 7.07 (dd, $J = 1.0$, 7.5 Hz, 2H), 7.03–7.01 (m, 2H), 6.95–6.94 (m, 1H), 6.87 ppm (d, $J = 8.5$ Hz, 2H); ¹³C NMR (CDCl₃, 125 MHz): $\delta = 190.4$, 154.3, 148.3, 145.8, 140.4, 139.8, 138.8, 131.6, 131.24, 131.17, 131.0, 130.9, 130.4, 129.7, 129.3, 128.7, 128.3, 128.20, 128.16, 128.1, 127.8, 127.6, 127.4, 127.3, 127.2, 127.1, 126.5, 126.4, 126.3, 126.23, 126.19, 126.1, 125.7, 125.5, 125.4, 125.2, 124.8, 124.7, 123.2, 122.8, 122.7, 122.0, 117.0, 112.4 ppm.

Synthesis of 4-((4'-phenyl(pyren-1-yl)amino)biphenyl-4-yl)(pyren-1-yl)amino)benzaldehyde (**2b**)

2b was obtained in 29% yield as a yellow solid from N^4, N^4 -diphenyl- N^4, N^4 -di(pyren-1-yl)biphenyl-4,4'-diamine by following a procedure similar to that described above for **2a**. M.p. 196–198 °C; IR (KBr): $\tilde{\nu}_{C=O} = 1685$ cm⁻¹; ¹H NMR (CDCl₃, 500 MHz): $\delta = 9.79$ (s, 1H), 8.22 (d, $J = 8.0$ Hz, 2H), 8.19–8.15 (m, 4H), 8.13–8.02 (m, 6H), 8.01–7.99 (m, 3H), 7.94 (d, $J = 9.5$ Hz, 1H), 7.88 (d, $J = 8.0$ Hz, 1H), 7.86 (d, $J = 8.0$ Hz, 1H), 7.67–7.65 (m, 2H), 7.49–7.47 (m, 2H), 7.40–7.38 (m, 2H), 7.30–7.28 (m, 2H), 7.24–7.21 (m, 2H), 7.13–7.12 (m, 2H), 7.09–7.08 (m, 2H), 6.99–6.97 ppm (m, 3H); ¹³C NMR (CDCl₃, 125 MHz): $\delta = 190.5$, 153.9, 148.3, 148.0, 145.1, 140.6, 138.8, 136.9, 133.2, 131.6, 131.24, 131.16, 131.1, 130.9, 130.5, 129.7, 129.3, 128.80, 128.75, 128.3, 128.2, 128.0, 127.8, 127.7, 127.6, 127.5, 127.4, 127.2, 127.1, 126.5, 126.4, 126.3, 126.2, 126.1, 125.7, 125.6, 125.3, 125.2, 125.1, 124.8, 124.7, 123.3, 122.6, 122.5, 122.2, 121.9, 118.2 ppm.

Synthesis of 4-((9,9-diethyl-7-phenyl(pyren-1-yl)amino)-9*H*-fluorene-2-yl)(pyren-1-yl)amino)benzaldehyde (**2c**)

2c was obtained in 20% yield as a yellow solid from 9,9-diethyl- N^2, N^7 -diphenyl- N^2, N^7 -di(pyren-1-yl)-9*H*-fluorene-2,7-diamine by following a procedure similar to that described above for **2a**. M.p. 220–222 °C; IR (KBr): $\tilde{\nu}_{C=O} = 1685$ cm⁻¹; ¹H NMR (CDCl₃, 500 MHz): $\delta = 9.78$ (s, 1H), 8.22–8.20 (m, 2H), 8.18–8.15 (m, 3H), 8.13–8.08 (m, 5H), 8.06 (s, 2H), 8.02–7.97 (m, 3H), 7.89–7.83 (m, 3H), 7.65 (d, $J = 8.5$ Hz, 2H), 7.47 (d, $J = 8.0$ Hz, 1H), 7.42 (d, $J = 8.5$ Hz, 1H), 7.28 (d, $J = 1.5$ Hz, 1H), 7.21 (t, $J = 7.5$ Hz, 2H), 7.10–7.07 (m, 4H), 6.96–6.93 (m, 4H), 1.81–1.72 (m, 4H), 0.35 ppm (t, $J = 7.25$ Hz, 6H); ¹³C NMR (CDCl₃, 125 MHz): $\delta = 190.5$, 154.4, 151.53, 151.46, 148.9, 148.2, 144.9, 141.2, 139.2, 138.5, 131.6, 131.3, 131.2, 131.1, 130.9, 130.2, 129.4, 129.2, 128.54, 128.47, 127.9, 127.8, 127.7, 127.32, 127.25, 127.2, 127.0, 126.5, 126.4, 126.3, 126.23, 126.15, 126.0, 125.7, 125.5, 125.2, 125.1, 124.9, 124.4, 123.5, 122.8, 122.1, 121.7, 120.2, 120.0, 119.8, 118.0, 117.1, 56.2, 32.6, 8.6 ppm.

Synthesis of (E)-2-cyano-3-4-((4-phenyl(pyren-1-yl)amino)phenyl)acrylic acid (**3a**)

A mixture of **2a** (1.38 g, 2 mmol), cyanoacetic acid (0.21 g, 2.48 mmol), ammonium acetate (53 mg, 0.69 mmol), and glacial acetic acid (25 mL) was heated under reflux for 12 h during which time the aldehyde **2a** was completely consumed as indicated by TLC. Cooling the reaction mixture to room temperature produced a red precipitate, which was filtered and washed with water and a diethyl ether/hexanes mixture (1:1) successively. The analytically pure product was obtained by recrystallization from a toluene/hexanes mixture (1:3, 20 mL) as a red solid; yield 1.29 g (85%); m.p. 220–222 °C; IR (KBr): $\tilde{\nu}_{C=N} = 2208$ cm⁻¹; ¹H NMR (CDCl₃, 500 MHz): $\delta = 8.39$ (d, $J = 8.0$ Hz, 1H), 8.35–8.32 (m, 2H), 8.29 (t, $J = 7.75$ Hz, 2H), 8.24–8.22 (m, 3H), 8.17–8.15 (m, 3H), 8.11–8.04 (m, 6H), 7.99 (d, $J = 8.0$ Hz, 2H), 7.88 (d, $J = 8.0$ Hz, 1H), 7.81 (d, $J = 9.0$ Hz, 2H),

7.25–7.20 (m, 4H), 6.98 (d, $J=9.0$ Hz, 4H), 6.94 (t, $J=7.5$ Hz, 1H), 6.76 ppm (d, $J=9.0$ Hz, 2H); ^{13}C NMR (CDCl_3 , 125 MHz): $\delta=152.3$, 148.3, 145.5, 140.4, 139.8, 138.8, 132.7, 131.14, 131.09, 130.9, 130.8, 130.3, 129.9, 129.7, 129.1, 128.5, 128.1, 128.02, 127.96, 127.6, 127.2, 127.1, 127.0, 126.9, 126.3, 126.0, 125.8, 125.7, 124.4, 124.3, 123.1, 123.0, 122.7, 122.4, 121.9, 117.3 ppm.

Synthesis of (E)-2-cyano-3-(4-((4'-(phenyl(pyren-1-yl)amino)biphenyl-4-yl)(pyren-1-yl)amino)phenyl)acrylic acid (3b)

Compound **3b** was prepared from **2b** by following a similar procedure as described for **3a**: brown solid; yield 60%; m.p. 257–262 °C; IR (KBr): $\tilde{\nu}_{\text{C}=\text{N}}=2216\text{ cm}^{-1}$; ^1H NMR (CDCl_3 , 500 MHz): $\delta=8.36$ – 8.28 (m, 4H), 8.23–8.17 (m, 6H), 8.11–8.01 (m, 6H), 7.92 (d, $J=8.0$ Hz, 2H), 7.85 (d, $J=8.5$ Hz, 1H), 7.77 (d, $J=8.5$ Hz, 2H), 7.49 (d, $J=8.5$ Hz, 2H), 7.42 (d, $J=8.5$ Hz, 2H), 7.25–7.18 (m, 4H), 7.01 (d, $J=8.0$ Hz, 2H), 6.98–6.92 (m, 3H), 6.87 ppm (d, $J=8.5$ Hz, 2H); ^{13}C NMR (CDCl_3 , 125 MHz): $\delta=148.1$, 140.5, 132.1, 131.1, 130.9, 130.0, 129.8, 128.6, 128.2, 128.1, 127.7, 127.2, 127.1, 126.9, 126.0, 125.8, 124.7, 124.3, 123.1, 122.7, 122.5, 121.7, 119.0 ppm; HRMS m/z : calcd for $\text{C}_{60}\text{H}_{57}\text{N}_5\text{O}_2$ 854.2783 [$\text{M}+\text{Na}^+$]; found 854.2932.

Synthesis of (E)-2-cyano-3-(4-((9,9-diethyl-7-(phenyl(pyren-1-yl)amino)-9H-fluoren-2-yl)(pyren-1-yl)amino)phenyl)acrylic acid (3c)

Compound **3c** was prepared from **2c** by following a similar procedure as described for **3a**: red solid; yield 50%; m.p. 277–279 °C; IR (KBr): $\tilde{\nu}_{\text{C}=\text{N}}=2212\text{ cm}^{-1}$; ^1H NMR (CDCl_3 , 500 MHz): $\delta=8.36$ – 8.26 (m, 4H), 8.23–8.15 (m, 6H), 8.07–7.95 (m, 8H), 7.83 (d, $J=8.5$ Hz, 1H), 7.78 (d, $J=7.0$ Hz, 2H), 7.58–7.52 (m, 2H), 7.36 (s, 1H), 7.23–7.20 (m, 2H), 7.08–7.06 (m, 2H), 6.97–6.92 (m, 3H), 6.85–6.81 (m, 3H), 1.69–1.62 (m, 4H), 0.23–0.20 ppm (m, 6H); ^{13}C NMR (CDCl_3 , 125 MHz): $\delta=156.7$, 156.2, 153.6, 152.7, 145.8, 144.1, 142.7, 140.0, 136.0, 135.9, 135.6, 134.9, 134.6, 134.2, 132.4, 132.2, 131.8, 130.8, 130.7, 130.4, 129.2, 129.1, 127.0, 126.7, 125.8, 125.6, 123.2, 60.8, 36.8, 13.6 ppm; LRMS m/z : calcd for $\text{C}_{65}\text{H}_{45}\text{N}_5\text{O}_2$ 922.3 [$\text{M}+\text{Na}^+$]; found 922.2.

DSSC Fabrication and Measurements

A fluorine-doped SnO_2 conducting glass electrode (FTO, $7\ \Omega\ \text{sq}^{-1}$, transmittance ca. 80%) was first cleaned with a neutral cleaner and then washed with deionized water, acetone, and isopropyl alcohol, sequentially. The conducting surface of the FTO was treated with a solution of titanium tetraisopropoxide (1 g) in 2-methoxyethanol (3 g) to obtain a good mechanical contact between the conducting glass and TiO_2 film, as well as to isolate the conducting glass surface from the electrolyte. TiO_2 pastes were coated onto the treated conducting glass by using the doctor blade technique. To coat each TiO_2 layer, the dried TiO_2 film was gradually heated to 450 °C under an oxygen atmosphere and subsequently sintered at that temperature for 30 min. The TiO_2 photoanodes of the DSSCs employed in the experiments were composed of a 14 μm thick transparent TiO_2 layer and with a scattering layer of 4.5 μm thickness. After sintering at 450 °C and cooling to 80 °C, the TiO_2 film was immersed in a $3 \times 10^{-4}\text{ M}$ solution of dye at room temperature for 24 h. The standard ruthenium complex, N719, was dissolved in acetonitrile and *tert*-butyl alcohol (1:1) to make a reference dye solution. Various organic dye solutions were prepared in a mixing solvent containing acetonitrile, *tert*-butyl alcohol, and DMSO (1:1:3). The thus prepared TiO_2 /dye electrode was placed on a platinum-sputtered conducting glass electrode (ITO, $7\ \Omega\ \text{sq}^{-1}$), thus keeping the two electrodes separated by a 25 μm thick Surlyn. The two electrodes were then sealed by heating. A mixture of 0.1 M LiI, 0.6 M 1-propyl-2,3-dimethylimidazolium iodide (DMPPI), 0.05 M I_2 , and 0.5 M *tert*-butylpyridine (TBP) in 3-methoxypropionitrile (MPN)/MeCN (1:1) was used as the electrolyte. The electrolyte was injected into the gap between the electrodes by capillarity; the electrolyte-injecting hole was previously made in the counter electrode with a drilling machine, and the hole was sealed with hot-melt glue after the injection of the electrolyte.

The surface of the DSSC was covered by a mask with a light-illuminated area of 0.16 cm^2 and then illuminated by a class A quality solar simulator. Incident light intensity (100 mW cm^{-2}) was calibrated with a standard sili-

con cell. Photocurrent–voltage curves of the DSSCs were obtained with a potentiostat/galvanostat. The thickness of the TiO_2 film was judged by scanning electron microscopic images (SEM). For UV absorption spectra, dye molecules were coated on the TiO_2 films, and the corresponding spectra were obtained by using an UV/Vis spectrophotometer equipped with an integrating sphere. Electrochemical impedance spectra (EIS) were obtained from the potentiostat/galvanostat, equipped with a FRA2 module, under a constant light illumination of 100 mW cm^{-2} . The frequency range explored was 10 mHz to 65 kHz. The applied bias voltage was set at the open-circuit voltage of the DSSC between the ITO-Pt counter electrode and the FTO- TiO_2 dye working electrode, starting from the short-circuit condition; the corresponding alternating current (AC) amplitude was 10 mV. The impedance spectra were analyzed by using an equivalent circuit model. IPCE curves were obtained under short-circuit conditions. The light source was a class A quality solar simulator (PEC-L11, AM 1.5 G); light was focused through a monochromator onto the photovoltaic cell. The monochromator was incremented through the visible spectrum to generate the IPCE (λ) as defined by $\text{IPCE}(\lambda) = 1240 (J_{\text{sc}}/\lambda\phi)$, where λ is the wavelength, J_{sc} is the short-circuit photocurrent density (mA cm^{-2}) recorded with a potentiostat/galvanostat, and ϕ is the incident radiative flux (W m^{-2}) measured with an optical detector and a power meter.

Acknowledgements

KRJT is thankful to Department of Science and Technology, New Delhi, India for financial support (Ref. No. DST/TSG/ME/2010/27). K.-C.H acknowledges a grant-in-aid from National Science Council, Taiwan. N.K. is thankful to University Grants Commission, New Delhi, India for research fellowship.

- [1] a) *Organic Electronics: Materials, Manufacturing and Applications* (Ed.: H. Klauk), Wiley-VCH, Weinheim, 2006; b) P. Wang, S. M. Zakeeruddin, J. E. Moser, M. K. Nazeeruddin, T. Sekiguchi, M. Grätzel, *Nat. Mater.* **2003**, *2*, 402–407.
- [2] a) T. Kitamura, M. Ikeda, K. Shigaki, T. Inoue, N. A. Anderson, X. Ai, T. Lian, S. Yanagida, *Chem. Mater.* **2004**, *16*, 1806–1812; b) S. Ito, S. M. Zakeeruddin, R. Humphry-Baker, P. Liska, R. Charvet, P. Comte, M. K. Nazeeruddin, P. Péchy, M. Takata, H. Miura, S. Uchida, M. Grätzel, *Adv. Mater.* **2006**, *18*, 1202–1205.
- [3] a) D. Heredia, J. Natera, M. Gervaldó, L. Otero, F. Fungo, C.-H. Lin, K.-T. Wong, *Org. Lett.* **2010**, *12*, 12–15; b) S.-H. Lin, Y.-C. Hsu, J. T. Lin, C.-K. Lin, J.-S. Yang, *J. Org. Chem.* **2010**, *75*, 7877–7886; c) S. Kim, J. K. Lee, S. O. Kang, J. Ko, J.-H. Yum, S. Fantacci, F. D. Angelis, D. D. Censo, M. K. Nazeeruddin, M. Grätzel, *J. Am. Chem. Soc.* **2006**, *128*, 16701–16707; d) Z. Ning, Q. Zhang, W. Wu, H. Pei, B. Liu, H. Tian, *J. Org. Chem.* **2008**, *73*, 3791–3797.
- [4] a) J. N. Clifford, E. Martínez-Ferrero, A. Viterisi, E. Palomares, *Chem. Soc. Rev.* **2011**, *40*, 1635–1646; b) A. Hagfeldt, G. Boschloo, L. C. Sun, L. Kloo, H. Pettersson, *Chem. Rev.* **2010**, *110*, 6595–6663; c) D. Venkataraman, S. Yurt, B. H. Venkataraman, N. Gavvalapalli, *J. Phys. Chem. Lett.* **2010**, *1*, 947–958; d) A. W. Hains, Z. Liang, M. A. Woodhouse, B. A. Gregg, *Chem. Rev.* **2010**, *110*, 6689–6735; e) C. Li, M. Liu, N. G. Pschirer, M. Baumgarten, K. Müllen, *Chem. Rev.* **2010**, *110*, 6817–6855; f) Y.-J. Cheng, S.-H. Yang and C.-S. Hsu, *Chem. Rev.* **2009**, *109*, 5868–5923; g) A. Mishra, M. K. R. Fischer, P. Bauerle, *Angew. Chem.* **2009**, *121*, 2510–2536; *Angew. Chem. Int. Ed.* **2009**, *48*, 2474–2499; h) Y. Ooyama, Y. Harima, *Eur. J. Org. Chem.* **2009**, 2903–2934.
- [5] a) Y. J. Chang, T. J. Chow, *Tetrahedron* **2009**, *65*, 4726–4734; b) A. Baheti, P. Tyagi, K. R. J. Thomas, Y. C. Hsu, J. T. Lin, *J. Phys. Chem. C* **2009**, *113*, 8541–8547.
- [6] a) W. Li, Y. Wu, X. Li, Y. Xie, W. Zhu, *Energy Environ. Sci.* **2011**, *4*, 1830–1837; b) C.-H. Chen, Y.-C. Hsu, H.-H. Chou, K. R. J. Thomas, J. T. Lin, C.-P. Hsu, *Chem. Eur. J.* **2010**, *16*, 3184–3193; c) J. T. Lin,

- P.-C. Chen, Y.-S. Yen, Y.-C. Hsu, H.-H. Chou, M. C. P. Yeh, *Org. Lett.* **2009**, *11*, 97–100; d) G. Zhou, N. Pschirer, J. C. Schoneboom, F. Eickemeyer, M. Baumgarten, K. Müllen, *Chem. Mater.* **2008**, *20*, 1808–1815; e) S.-T. Huang, Y.-C. Hsu, Y.-S. Yen, H.-H. Chou, J. T. Lin, C.-W. Chang, C.-P. Hsu, C. Tsai, D.-J. Yin, *J. Phys. Chem. C* **2008**, *112*, 19739–19747; f) K. R. J. Thomas, J. T. Lin, Y.-C. Hsu, K.-C. Ho, *Chem. Commun.* **2005**, 4098–4100.
- [7] a) P. Shen, Y. Tang, S. Jiang, H. Chen, X. Zheng, X. Wang, B. Zhao, S. Tan, *Org. Electron.* **2011**, *12*, 125–135; b) C.-H. Yang, S.-H. Liao, Y.-K. Sun, Y.-Y. Chuang, T.-L. Wang, Y.-T. Shieh, W.-C. Lin, *J. Phys. Chem. C* **2010**, *114*, 21786–21794; c) C. Zafer, B. Gultekin, C. Ozsoy, C. Tozlu, B. Aydin, S. Icli, *Solar Energy Mater. Solar Cells* **2010**, *94*, 655–661; d) K. Hara, Z. S. Wang, Y. Cui, A. Furube, N. Koumura, *Energy Environ. Sci.* **2009**, *2*, 1109–1114; e) C. Teng, X.-C. Yang, C.-Z. Yuan, C.-Y. Li, R. Chen, H. Tian, S. Li, A. Hagfeldt, L. Sun, *Org. Lett.* **2009**, *11*, 5542–5545; f) N. Koumura, Z.-S. Wang, M. Miyashita, Y. Uemura, H. Sekiguchi, Y. Cui, A. Mori, S. Mori, K. Hara, *J. Mater. Chem.* **2009**, *19*, 4829–4836; g) N. Koumura, Y. Cui, M. Takahashi, H. Sekiguchi, A. Furube, K. Hara, *Chem. Mater.* **2008**, *20*, 3993–4003; h) D. Kim, J. K. Lee, S. O. Kang, J. Ko, *Tetrahedron* **2007**, *63*, 1913–1922.
- [8] a) M. K. R. Fischer, S. Wenger, M.-K. Wang, A. Mishra, S. M. Zakeeruddin, M. Grätzel, P. Bauerle, *Chem. Mater.* **2010**, *22*, 1836–1845; b) R. Z. Li, X. J. Lv, D. Shi, D. F. Zhou, Y. M. Cheng, G. L. Zhang, P. Wang, *J. Phys. Chem. C* **2009**, *113*, 7469; c) K. R. J. Thomas, Y.-C. Hsu, J. T. Lin, K.-M. Lee, K.-C. Ho, C.-H. Lai, Y.-M. Cheng, P.-T. Chou, *Chem. Mater.* **2008**, *20*, 1830–1840; d) W. H. Liu, I. C. Wu, C. H. Lai, P. T. Chou, Y. T. Li, C. L. Chen, Y. Y. Hsu, Y. Chi, *Chem. Commun.* **2008**, 5152–5154.
- [9] a) D. Xiao, L. A. Martini, R. C. Snoeberger, R. H. Crabtree, V. S. Batista, *J. Am. Chem. Soc.* **2011**, *133*, 9014–9022; b) S. Agrawal, P. Dev, N. J. English, K. R. Thampi, J. M. D. MacElroy, *J. Mater. Chem.* **2011**, *21*, 11101–11108; c) S. E. Koops, P. R. F. Barnes, B. C. O'Regan, J. R. Durrant, *J. Phys. Chem. C* **2010**, *114*, 8054–8061; d) Z.-S. Wang, Y. Cui, Y. Dan-Oh, C. Kasada, A. Shinpo, K. Hara, *J. Phys. Chem. C* **2007**, *111*, 7224–7230; e) Z.-S. Wang, Y. Cui, K. Hara, Y. Dan-Oh, C. Kasada, A. Shinpo, *Adv. Mater.* **2007**, *19*, 1138–1141.
- [10] a) A. Baheti, P. Singh, C.-P. Lee, K. R. J. Thomas, K.-C. Ho, *J. Org. Chem.* **2011**, *76*, 4910–4920; b) H. Choi, I. Raabe, D. Kim, F. Teocoli, C. Kim, K. Song, J.-H. Yum, J. Ko, M. K. Nazeeruddin, M. Grätzel, *Chem. Eur. J.* **2010**, *16*, 1193–1201; c) C. Kim, H. Choi, S. Kim, C. Baik, K. Song, M.-S. Kang, S.-O. Kang, J. Ko, *J. Org. Chem.* **2008**, *73*, 7072–7079; d) H. Choi, J.-K. Lee, K. Song, S.-O. Kang, J. Ko, *Tetrahedron* **2007**, *63*, 3115–3121.
- [11] a) J. He, W. Wu, J. Hua, Y. Jing, S. Qu, J. Li, Y. Long, H. Tian, *J. Mater. Chem.* **2011**, *21*, 6054–6062; b) H.-Y. Yang, Y.-S. Yen, Y.-C. Hsu, H.-H. Chou, J. T. Lin, *Org. Lett.* **2010**, *12*, 16–19; c) M.-F. Xu, S. Wenger, H. Bala, D. Shi, R.-Z. Li, Y.-Z. Zhou, S. M. Zakeeruddin, M. Grätzel, P. Wang, *J. Phys. Chem. C* **2009**, *113*, 2966–2973; d) G.-L. Zhang, Y. Bai, R.-Z. Li, D. Shi, S. Wenger, S. M. Zakeeruddin, M. Grätzel, P. Wang, *Energy Environ. Sci.* **2009**, *2*, 92–95; e) Y.-S. Yen, Y.-C. Hsu, J. T. Lin, C.-W. Chang, C.-P. Hsu, D.-J. Yin, *J. Phys. Chem. C* **2008**, *112*, 12557–12567; f) H. Qin, S. Wenger, M. Xu, F. Gao, X. Jing, P. Wang, S. M. Zakeeruddin, M. Grätzel, *J. Am. Chem. Soc.* **2008**, *130*, 9202–9204.
- [12] D. Kumar, K. R. J. Thomas, C.-P. Lee, K.-C. Ho, *Org. Lett.* **2011**, *13*, 2622–2625.
- [13] M.-S. Tsai, Y.-C. Hsu, J. T. Lin, H.-C. Chen, C.-P. Hsu, *J. Phys. Chem. C* **2007**, *111*, 18785–18793.
- [14] M. Velusamy, Y.-C. Hsu, J. T. Lin, C.-W. Chang, C.-P. Hsu, *Chem. Asian J.* **2010**, *5*, 87–96.
- [15] A. Baheti, C.-P. Lee, K. R. J. Thomas, K.-C. Ho, *Phys. Chem. Chem. Phys.* **2011**, *13*, 17210–17221.
- [16] M.-W. Lee, S.-B. Cha, S.-J. Yang, S.-W. Park, K. Kim, N.-G. Park, D.-H. Lee, *Bull. Korean Chem. Soc.* **2009**, *30*, 2269–2279.
- [17] Y. S. Wong, Y. S. Yang, J. H. Kim, J.-H. Ryu, K. K. Kim, S. S. Park, *Energy Fuels* **2010**, *24*, 3676–3681.
- [18] S.-L. Lai, Q.-X. Tong, M.-Y. Chan, T.-W. Ng, M.-F. Lo, S.-T. Lee, C.-S. Lee, *J. Mater. Chem.* **2011**, *21*, 1206–1211.
- [19] S. Ji, W. Wu, W. Wu, P. Song, K. Han, Z. Wang, S. Liu, H. Guo, J. Zhao, *J. Mater. Chem.* **2010**, *20*, 1953–1963.
- [20] S. L. Lai, Q. X. Tong, M. Y. Chan, T. W. Ng, M. F. Lo, C. C. Ko, S. T. Lee, C. S. Lee, *Org. Electron.* **2011**, *12*, 541–546.
- [21] a) K. R. J. Thomas, M. Velusamy, J. T. Lin, C.-H. Chuen, Y.-T. Tao, *J. Mater. Chem.* **2005**, *15*, 4453–4459; b) K. R. J. Thomas, J. T. Lin, Y.-T. Tao, C.-W. Ko, *J. Am. Chem. Soc.* **2001**, *123*, 9404–9411.
- [22] a) L. Zöphel, V. Enkelmann, R. Rieger, K. Müllen, *Org. Lett.* **2011**, *13*, 4506–4509; b) P. Sonar, M. S. Soh, Y. H. Cheng, J. T. Henssler, A. Sellinger, *Org. Lett.* **2010**, *12*, 3292–3295.
- [23] a) A. Nantalaksakul, A. Mueller, A. Klaiherd, C. J. Bardeen, S. Thayumanavan, *J. Am. Chem. Soc.* **2009**, *131*, 2727–2738; b) K. R. J. Thomas, A. L. Thompson, A. V. Sivakumar, C. J. Bardeen, S. Thayumanavan, *J. Am. Chem. Soc.* **2005**, *127*, 373–383.
- [24] a) H. Tian, X. Yang, J. Pan, R. Chen, M. Liu, Q. Zhang, A. Hagfeldt, L. Sun, *Adv. Funct. Mater.* **2008**, *18*, 3461–3468; b) G. Li, Y.-F. Zhou, X.-B. Cao, P. Bao, K.-J. Jiang, Y. Lin, L.-M. Yang, *Chem. Commun.* **2009**, 2201–2203.
- [25] a) J. Tang, J. Hua, W. Wu, J. Li, Z. Jin, Y. Long, H. Tian, *Energy Environ. Sci.* **2010**, *3*, 1736–1745; b) L. Zhang, Y. Liu, Z. Wang, M. Liang, Z. Sun, S. Xue, *Tetrahedron* **2010**, *66*, 3318–3325.
- [26] J. F. Hartwig, *Angew. Chem.* **1998**, *110*, 2154–2177; *Angew. Chem. Int. Ed.* **1998**, *37*, 2046–2067.
- [27] B. E. Koene, D. E. Loy, M. E. Thompson, *Chem. Mater.* **1998**, *10*, 2235–2250.
- [28] Gaussian 09, Revision A.02, M. J. Frisch, G. W. Trucks, H. B. Schlegel, G. E. Scuseria, M. A. Robb, J. R. Cheeseman, G. Scalmani, V. Barone, B. Mennucci, G. A. Petersson, H. Nakatsuji, M. Caricato, X. Li, H. P. Hratchian, A. F. Izmaylov, J. Bloino, G. Zheng, J. L. Sonnenberg, M. Hada, M. Ehara, K. Toyota, R. Fukuda, J. Hasegawa, M. Ishida, T. Nakajima, Y. Honda, O. Kitao, H. Nakai, T. Vreven, J. A., Jr., Montgomery, J. E. Peralta, F. Ogliaro, M. Bearpark, J. J. Heyd, E. Brothers, K. N. Kudin, V. N. Staroverov, R. Kobayashi, J. Normand, K. Raghavachari, A. Rendell, J. C. Burant, S. S. Iyengar, J. Tomasi, M. Cossi, N. Rega, N. J. Millam, M. Klene, J. E. Knox, J. B. Cross, V. Bakken, C. Adamo, J. Jaramillo, R. Gomperts, R. E. Stratmann, O. Yazyev, A. J. Austin, R. Cammi, C. Pomelli, J. W. Ochterski, R. L. Martin, K. Morokuma, V. G. Zakrzewski, G. A. Voth, P. Salvador, J. J. Dannenberg, S. Dapprich, A. D. Daniels, Ö. Farkas, J. B. Foresman, J. V. Ortiz, J. Cioslowski, D. J. Fox, Gaussian, Inc., Wallingford, CT, **2009**.

Received: October 13, 2011

Published online: February 1, 2012